Suppressing Co-ion Generation via Cationic Proton Donors to Amplify Driving

Forces for Electrochemical CO₂ Reduction

Wenxiao Guo, † Beichen Liu, † Matthew A. Gebbie †*

†Department of Chemical and Biological Engineering, University of Wisconsin-Madison, Madison, Wisconsin

53706, United States

*Address correspondence to gebbie@wisc.edu

Keywords: Electrocatalysis, ionic liquids, electric double layer, interfaces, CO₂ reduction

Abstract

Interfacial microenvironments critically define reaction pathways for electrocatalytic processes through

a combination of electric field gradients and proton activity. Non-aqueous ionic liquid electrolytes have

been shown to sustain enhanced interfacial electric field gradients at intermediate ion concentration regimes

of around 1 M, creating local environments that promote CO₂ electroreduction. Notably, water at low

concentrations absorbed by non-aqueous electrolytes is usually assumed to be the proton donor for CO₂

reduction. Consumption of protons causes proton donors to become more negative by one unit charge,

which significantly modifies the local concentration of charged species and hence should strongly impact

local electric fields. Yet, how the coupling between proton donation and changing interfacial electric fields

influences electrocatalytic processes in non-aqueous electrolytes remains largely unexplored. In this work,

we show that the high activity of 1,3-dialkylimidazolium ionic liquids for CO₂ reduction in acetonitrile-

based electrolytes stems from the ability to act as cationic proton donors that release neutral conjugate bases.

Using in situ electrochemical surface-enhanced Raman spectroscopy, we find that the formation of neutral

conjugate bases from imidazolium cations preserves local electric field strengths at electrode-electrolyte

interfaces, providing a powerful strategy to maintain an active local microenvironment for CO₂ reduction.

In contrast, conditions where water behaves as the primary proton donor generates [OH] anions as negative

"co-ions" in the electric double layer, which weakens the interfacial electric field and significantly

compromises the steady-state CO₂ reduction activity. Our study highlights that electrochemical driving

forces are highly sensitive to the charge state of both reactant and product species and highlights the fact

that the generation of interfacial co-ions plays a key role in determining electrochemical driving forces.

1

Introduction

Electrochemical reduction of CO₂ to chemical fuels has received heightened research interest motivated by the growing need to mitigate global warming and develop sustainable replacements for fossil fuels in chemical synthesis. ¹⁻⁷ Interfacial microenvironments exhibit distinct properties from bulk electrolytes, and these local properties, such as altered interfacial ion concentrations, often play defining in controlling reaction pathways during electrochemical processes. In recent years, growing research efforts have focused on understanding and tuning interfacial microenvironments through electrolyte engineering. ^{8,9} For example, local concentration of cations at electrode-electrolyte interface was shown to increase at higher electrolyte alkalinity and more negative applied potential, which consequentially modifies interfacial electric field, adsorption energy of key intermediates, and eventually the rate and selectivity of electrochemical reactions such as hydrogen evolution and CO₂ reduction. ¹⁰⁻¹³

Most studies of CO₂ electroreduction focus on the reduction of CO₂ in aqueous electrolytes due to the accessibility and environmentally benign nature of water. ¹⁴⁻¹⁷ Further, water acts as a proton donor that is necessary for proton-coupled electron transfers in electrochemical reduction of CO₂, including the two-electron reduction of CO₂ to CO. However, the competing hydrogen evolution reaction in aqueous systems often compromises the selectivity towards CO₂ reduction.

One strategy to enhance the efficiency of CO₂ electroreduction is to circumvent hydrogen evolution by conducting CO₂ electroreduction in non-aqueous systems. ¹⁸⁻²³ Ionic liquids are especially promising salts for CO₂ electroreduction, as ionic liquids can facilitate especially high rates of selective CO₂ electroreduction at record low overpotentials in both aqueous and non-aqueous electrolytes. ²⁴⁻²⁹ Ionic liquids are salts composed of organic cations and either inorganic or organic anions, which provide a wide parameter space of possible properties that can be designed to study and control electrochemical processes. ³⁰⁻³⁵ Further, ionic liquids have high electrochemical stability and provide ionic conductivity to organic solvents, ^{36,37} eliminating the need to include additional salt species to mitigate solution resistance.

One of the most widely studied categories of ionic liquids in electrochemical CO₂ reduction is ionic liquids with imidazolium-derived cations. ³⁸⁻⁴⁴ Since the first report of using a 1,3-diakylimidazolium ionic liquid for CO₂ reduction to CO with unprecedently low overpotential, ²⁶ tremendous discussions were invoked to understand how imidazolium cations accelerate CO₂ reduction. Early studies proposed that imidazolium species acted as co-catalysts by being first reduced to carbenes, which coordinate with CO₂ to form imidazolium-CO₂ adducts that were believed to be more readily reduced to CO. ^{39,42} However, more recent studies suggest that higher reactivity of CO₂ reduction can be achieved using trialkylimidazolium cations such as 1-ethyl-2,3-dimethylimidazolium whose C2 position is blocked to prevent the formation of carbenes and adducts. ^{24,25} These studies were interpreted as suggesting that imidazolium-CO₂ adducts are

inactive side products from CO_2 reduction, and the function of imidazolium cations was interpreted as the stabilization of intermediate CO_2 radicals by imidazolium cations via non-covalent interactions.

While improved understanding of the interaction between individual imidazolium cations and CO₂ set up the foundation to optimize electrolytes composed of imidazolium-based cations for CO₂ reduction, recent studies showed that collective, multi-ion correlations between clusters of cations and anions provide additional dimensions to tune the reactivity of CO₂ reduction in ionic liquid electrolytes. Specifically, our group previously demonstrated that the reactivity and selectivity of CO₂ reduction to CO in 1-ethyl-3-methylimidazolium tetrafluoroborate ([EMIm][BF₄])-acetonitrile electrolytes were drastically enhanced at intermediate concentrations of [EMIm][BF₄] at around 1 M due to enhanced screening and larger interfacial electric field in electric double layers, which stabilizes charged CO₂- intermediates. ⁴⁵

Notably, the 1-ethyl-2,3-dimethylimidazolium ([EMMIm][BF₄]) ionic liquid, which was reported to exhibit higher reactivity for CO₂ reduction than [EMIm][BF₄] at low concentrations and low applied overpotentials, failed to maintain high reactivity at intermediate concentrations during steady-state electrolysis. This was found to originate from the formation of high interfacial concentrations of negative (bi)carbonate co-ions during CO₂ reduction when using the intrinsic moisture (water) as the proton source, which releases [OH]⁻ that combines with CO₂ to form (bi)carbonates.

Importantly, the rapid buildup of (bi)carbonates leads to nucleation and growth of [EMMIm][HCO₃] crystals that passivate the surface of electrode. ⁴⁵ Similar electrode deactivation due to (bi)carbonate buildup is also frequently reported in CO₂ electroreduction using inorganic salt electrolytes. ^{46,47} Together, these observations suggest that negative co-ions generated due to proton donation during CO₂ reduction and their correlations with cations greatly impact the overall performance of electrolytes, an aspect that is often overlooked. More importantly, the absence of similar surface passivation by bi(carbonate) generation in [EMIm][BF₄]-based electrolytes strongly suggests that a gap exists in the understanding of roles played by dialkylimidazolium cations with C2 protons (C2-H) in maintaining the activity of electrode-electrolyte interfaces in non-aqueous electrolytes.

In this work, we study CO₂ electrochemical reduction in 0.7 M [EMIm][BF₄]-acetonitrile electrolytes with varied water concentrations as a model. We evaluate how imidazolium cations with C2-H influence CO₂ reduction by simultaneously donating protons to CO₂ in proton-coupled electron transfers and mitigating the formation of surface-passivating co-ions [OH]⁻/[HCO₃]⁻ by forming [EMIm-CO₂] adducts. We first demonstrate the role of [EMIm]⁺ as a proton donor by using kinetic isotope effect studies to show a decrease in CO₂ reduction rate in [EMIm][BF₄]-acetonitrile electrolytes when the C2 position of the imidazolium ring is deuterated ([D-EMIm]⁺). We then compare the short-term kinetics and long-term steady-state activity of CO₂ reduction when either [EMIm]⁺ or water acts as primary proton donors. By

observing the faster short-term kinetics but lower long-term CO₂ reduction activity when water becomes the dominating proton donor, we highlight the advantage of sourcing protons from positive donors such as imidazolium cations and releasing neutral conjugate base such as [EMIm-CO₂] in CO₂ reduction.

Ultimately, we find that while [EMIm-CO₂] does not directly facilitate the reduction of CO₂, sourcing protons from cationic species maintains strong interfacial electric field gradients and prevents the undesirable interaction between unreacted [EMIm]⁺ and anionic co-ions that would occur when a neutral proton donor such as water is adopted. Both effects provide a local interfacial microenvironment favorable to CO₂ electroreduction. Taken together, our new understandings of the dual function of imidazolium cations in electrochemical CO₂ reduction provides critical insights into the design and optimization of organic electrolytes for carbon upgrading operated at high current densities.

Results and Discussion

Imidazolium acts as a proton donor in CO₂ reduction.

The role played by the C2 position of imidazolium cations in electrochemical CO₂ reduction is under active discussion. ^{40,41} Imidazolium cations are known to form moderately stable N-heterocyclic carbenes (NHCs) that catalyze a wide range of inorganic and organic reactions by forming coordinating complexes. ^{48,49} Hence, discussions on the mechanism behind imidazolium-catalyzed electrochemical CO₂ reduction often focus on the possible coordination of imidazolium NHCs to CO₂ molecules and the formation of imidazolium-COO as an active intermediate. ^{41,50,51} Yet, in many cases, the fate of C2-Hs and how they are involved in the overall reaction path is often overlooked.

Proton donors are increasingly emphasized as playing critical roles in facilitating and defining mechanisms of low overpotential electrochemical CO₂ reduction through proton-coupled electron transfers. ^{21,52-55} Prior studies of electrochemical CO₂ reduction in non-aqueous electrolytes usually attributed the proton donors to either trace amount of impurity water or water manually added to the electrolyte. ^{21,45,51} The overall reaction equation is assumed as:

$$CO_2 + H_2O + 2e^- \rightarrow CO + 2OH^-$$
 (Eq. 1)

Yet, we measured changes in water concentration following steady-state [EMIm][BF₄]-facilitated electrochemical CO₂ reduction and found that instead of being consumed, water was generated during electrolysis (Table S1). Our findings are consistent with our prior work that also observed electrochemical generation of water during ionic liquid-mediated CO₂ electroreduction in acetonitrile electrolytes with trace water content. ⁴⁵ This observation indicates that protons involved in CO₂ reduction are from alternative donors in the electrolytes, such as imidazolium cations, and water was released as a side product. While the C2-H of imidazolium cations possess a low acidity and is generally not considered an efficient proton donor

in CO₂ reduction, we found that fast deuteration of [EMIm]⁺ at the C2 position in D₂O occurred under weakly alkaline condition (pD 8), indicating that C2-H undergoes rapid proton exchange with surrounding water in the presence of nucleophiles such as [OH]⁻ or even CO₂⁻ (Fig. S1). Therefore, we propose that imidazolium cations with exposed C2-H (i.e., no alkylation at C2 position) readily act as proton donors of electrochemical CO₂ reduction by donating the C2-H, particularly in cathodic interfacial environments.

To further understand how the C2-H of imidazolium cations is involved in CO₂ reduction, we analyzed how the kinetics of CO₂ reduction in an [EMIm]BF₄]-acetonitrile electrolyte changed when the C2-H of [EMIm]⁺ was deuterated ([D-EMIm][BF₄], Fig. S2). Noticing that the D₂O-based deuteration and purification procedures may also impact the activity of [EMIm][BF₄], we treated [EMIm][BF₄] through same procedures but using regular water for a more rigorous comparison (denoted as [H-EMIm][BF₄] to separate from untreated [EMIm][BF₄]). We compared the performance of electrochemical CO₂ reduction in 0.7 M [H-EMIm][BF₄] and [D-EMIm][BF₄] in acetonitrile. A polycrystalline Ag (pc-Ag) disk electrode that is known to have high selectivity of CO in CO₂ reduction was used as the working electrode, providing a platform for model study. The concentration was set to 0.7 M as this concentration resided in the intermediate concentration regime, which can enhance reactivity by achieving stronger screening at the electrode-electrolyte interface.

Linear sweep voltammetry of CO₂ reduction in [H-EMIm][BF₄] and [D-EMIm][BF₄]-acetonitrile showed a more cathodic onset potential of [D-EMIm][BF₄] (Fig. 1A). During steady-state chronoamperometry (CA) electrolysis at -2.20, -2.35 and -2.50 V vs Ag/Ag⁺, the current density of CO₂ reduction decreased in [D-EMIm][BF₄] electrolyte compared with [H-EMIm][BF₄] electrolyte (Fig. 1B), while both electrolytes showed similar faradaic efficiencies toward CO at all applied potentials tested (Fig. 1B). The lowered faradaic efficiency at -2.20 V vs Ag/Ag⁺ can be attributed to the low total current density (around 1.0 mA/cm²), which exposed the presence of background electron transfer process that also occurred under Ar-purging (Fig. S3), most likely the formation of imidazolium carbene and H₂ at low kinetics (Fig. S4). Nonetheless, the similar faradaic efficiencies and lower current density of CO₂ reduction in [D-EMIm][BF₄] electrolyte at -2.35 and -2.50 V vs Ag/Ag⁺ compared with [H-EMIm][BF₄] indicated that the reaction mechanism remained the same in both electrolytes, while the deuteration of C2-H slowed the reaction kinetics. This kinetic isotope effect (KIE) indicates that deprotonation of C2-H is involved in the rate-determining step (RDS) of CO₂ reduction.

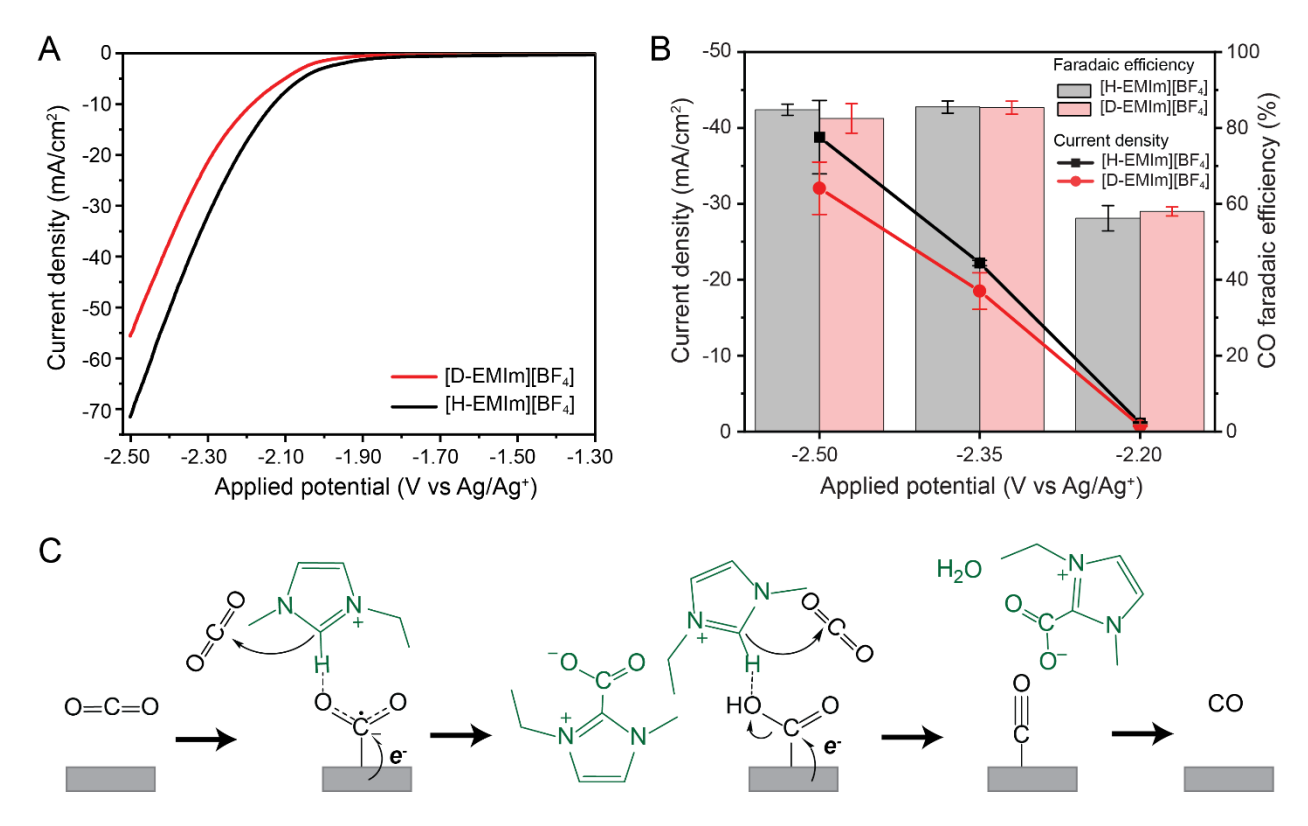


Figure 1. [EMIm]⁺ is a proton donor for CO₂ electroreduction in [EMIm][BF₄]-acetonitrile electrolytes. (A) Linear sweep voltammetry of 0.7 M [H-EMIm][BF₄]-acetonitrile (black) and 0.7 M [D-EMIm][BF₄]-acetonitrile (red) electrolytes saturated with CO₂ at 0.05 M water (intrinsic water concentration absorbed by the electrolyte). The [D-EMIm][BF₄]-acetonitrile electrolyte shows both a more cathodic onset potential and a lower overall current density for CO₂ reduction. (B) Average current density (lines, left axis) and faradaic efficiency of CO (bars, right axis) of CO₂ reduction in 0.7 M [H-EMIm][BF₄]-acetonitrile (black) and 0.7 M [D-EMIm][BF₄]-acetonitrile electrolytes at 0.05M water. At all applied potentials, [D-EMIm][BF₄] exhibited lower average current density but similar faradaic efficiency to CO compared with [H-EMIm][BF₄], indicating that deuterating C2-H leads to the same mechanism but lower activity, which confirms C2-H as a proton donor. (C) Proposed proton-coupled electron transfer pathway with [EMIm]⁺ as the proton donor in CO₂ reduction.

The donation of C2-H from [EMIm]⁺ to CO₂ yields unstable imidazolium carbenes as conjugate bases, which would immediately coordinate to a nearby electrophile, such as protons or dissolved CO₂ molecules. The coordination of imidazolium carbenes to protons regenerates [EMIm]⁺, while the coordination to CO₂ generates neutral [EMIm-CO₂] adducts as the converted conjugate base. We used ¹H nuclear magnetic resonance (NMR) analysis to confirm that [EMIm-CO₂] adducts formed in both [EMIm][BF₄] and [D-EMIm][BF₄] electrolytes (Fig. S5). Notably, the ratio between total amount of [EMIm-CO₂] and CO formed was around 1.65 (Table S2), which was close to the theoretical ratio of 2 between the number of proton

donors consumed and the number of CO generated in proton-coupled CO₂ reduction. We summarize the pathway of [EMIm]⁺-mediated CO₂ reduction in Figure 1C, and the full reaction equation is expressed as:

$$3CO_2 + 2[EMIm]^+ + 2e^- \rightarrow CO + 2[EMIm-CO_2] + H_2O$$
 (Eq. 2)

Noticing that zwitterionic [EMIm-CO₂] is a derivative of conjugate base that does not strongly correlate with [EMIm]⁺, we hypothesize that sourcing protons from [EMIm]⁺ avoids the excessive formation of [OH]⁻ or [HCO₃]⁻ and is hence critical for the outstanding performance of imidazolium-based ionic liquids in CO₂ reduction.

Kinetic analysis of [EMIm]⁺ and water-mediated CO₂ reduction.

To further demonstrate the importance of using [EMIm]⁺ as a proton donor, we systematically doped water into [EMIm][BF₄]-acetonitrile electrolytes as an alternative proton donor and analyzed how the performance of the electrolytes in CO₂ reduction changes. We anticipate that similar to the reported case of [EMMIm][BF₄], using water as a proton donor will enhance the immediate kinetics but compromise the steady-state activity during prolonged electrolysis.

We first studied the kinetics of CO₂ reduction at different water contents using linear sweep voltammetry (LSV) to justify water can outcompete [EMIm]⁺ as the proton donor in 0.7 M [EMIm][BF₄]-acetonitrile electrolytes. Figure 2A shows that by increasing the water concentration from 0.04 M (the intrinsic humidity of [EMIm][BF₄]-acetonitrile electrolyte) to over 1 M, the onset potential of CO₂ reduction moved anodically by about 0.1 V and the overall current density significantly increased. These results indicate that the immediate kinetics of CO₂ reduction indeed increased with water content, as water has lower acidity and is a more facile proton donor compared to [EMIm]⁺.

Tafel analysis further confirms the identity of dominating proton donors at different water concentrations (Fig. 2B). Prior studies on CO₂ reduction on pc-Ag electrodes in aqueous systems with water as proton donors suggested a theoretical Tafel slope of 118 mV/dec, in which the first proton-coupled electron transfer step is the RDS with a charge transfer coefficient of 0.5. ⁵⁶ Decreasing the acidity and increasing the size of proton donors in non-aqueous systems can result in a charge transfer coefficient significantly lower than 0.5 and consequentially a Tafel slope much higher than 118 mV/dec for a proton-coupled electron transfer step. ⁵⁷

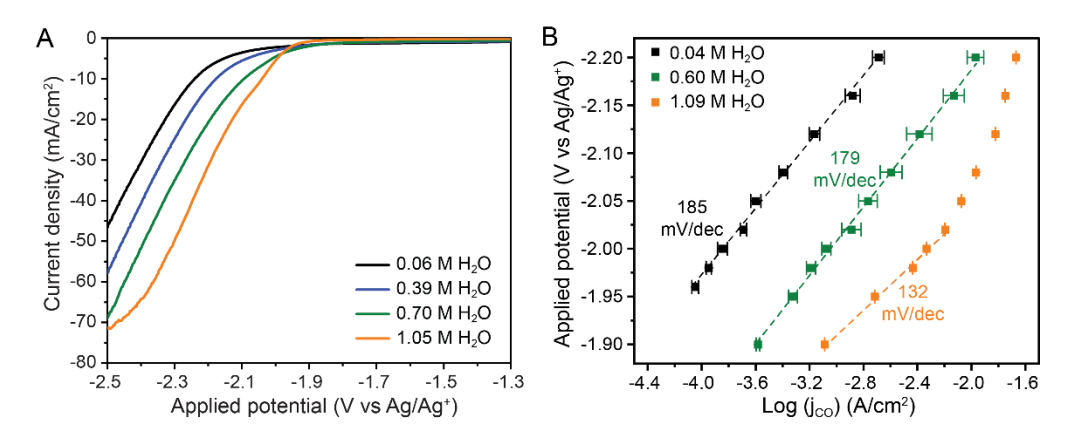


Figure 2. Kinetic studies of CO₂ reduction with [EMIm]⁺ and water acting proton donors. (A) Linear sweep voltammetry of CO₂ reduction in 0.7 M [EMIm][BF₄]-acetonitrile electrolytes doped with different concentrations of water. The onset potential shifts to less cathodic potentials and the current density grows higher when the water concentration increases. (B) Tafel plots of CO₂ reduction in 0.7 M [EMIm][BF₄]-acetonitrile electrolytes at representative water concentrations. When the water concentration increases, the Tafel slope gradually decreases from over 180 mV/dec to near 118 mV/dec, the theoretical value for proton-coupled CO₂ reduction in aqueous electrolytes.

We found that the Tafel slope of CO formation is about 185 mV/dec at 0.04 M water. The linearity of the slope across a wide potential range suggests that the large slope is unlikely a consequence of mass transport limit but is rather a result of the chemical properties of the proton donor. Therefore, the large Tafel slope supports the conclusion that [EMIm]⁺ was the primary proton donor. Increasing the water concentration from 0.04 M to 1.09 M caused the Tafel slope to gradually drop to 132 mV/dec, which suggests the emergence of another proton-coupled electron transfer pathway with a higher electron transfer coefficient, most likely water-mediated CO₂ reduction with water as the proton donor. Yet, the deviation of 132 mV/dec from both 185 mV/dec for [EMIm]⁺-mediated CO₂ reduction and the theoretical value of 118 mV/dec for water-mediated CO₂ reduction implies that [EMIm]⁺ and water coexist as proton donors under all cases studied. Meanwhile, the large nonlinearity of the Tafel slope at 1.09 M water under high overpotentials suggests that the system was subject to mass transport limitations due to the increased reaction kinetics, which may also exist at lower overpotentials and cause a higher apparent Tafel slope. ^{56,58} Further, the mass transport limitation of water-mediated CO₂ reduction may also contribute to the Tafel slope at 0.6 M water (179 mV/dec), which was close to the slope at 0.04 M water despite the participation of water as proton donors as reflected by LSV results (Fig. 2A).

Influence of proton donors and their conjugate bases on the steady-state reactivity.

We then performed CA experiments to analyze long-term activity of electrolytes doped with different water concentrations. Figure 3 shows the average steady-state total current densities and faradaic efficiencies of all products in 0.7 M [EMIm][BF4]-acetonitrile electrolytes at -2.20 and -2.35 V vs Ag/Ag⁺ with designated water concentrations. The range of water concentration and applied potentials are selected such that no significant degradation of electrolyte and hydrogen evolution occurred according to CV screening results (Fig. S6). Initial CA current densities averaged over the first 10 seconds increase with water concentrations (Fig. S7), which is a trend similar to that observed in kinetic studies (Fig. 2 and Fig. S6). However, we observed a significant drop in current densities over time for electrolytes with higher water concentrations during prolonged CA studies. Eventually, the average steady-state total current density and selectivity toward CO₂ reduction in 0.7 M [EMIm][BF4]-acetonitrile electrolytes monotonically decreases with increased water concentration at both -2.20 V and -2.35 V vs Ag/Ag⁺, which was opposite to the dependence of short-term kinetics on water concentrations. We verified that such a decrease was not due to the passivation of electrode surfaces by salt precipitation.

Figure 3 also shows that higher water concentrations promote the formation of formate and H₂. Moreover, a time-dependent analysis of product distributions (Fig. S8) showed that the decrease in CO selectivity and the increase in H₂ selectivity emerged only in later stage of steady-state electrolysis. Such a time dependence of overall activity and product selectivity is most likely a result of changes in interfacial microenvironment caused by side product buildup when water acts as the proton donor.

One main difference brought by switching from [EMIm]⁺ to water as the primary proton donor is the formation of [OH]⁻ instead of carbene as the conjugate base. Therefore, we attribute the decrease of CO₂ reduction activity and selectivity at increased water concentration to the accumulation of [OH]⁻ or [HCO₃]⁻ at electrode-electrolyte interface, which is expected to provide a contribution on interfacial electric field that works against the imposed potential on the electrode driving CO₂ reduction. Further, the stable CO₂ reduction reactivity in electrolytes with low water concentrations strongly indicates that using [EMIm]⁺ as the sole proton donor possesses an additional advantage in maintaining the activity and selectivity of electrolytes during long-term electrocatalysis.

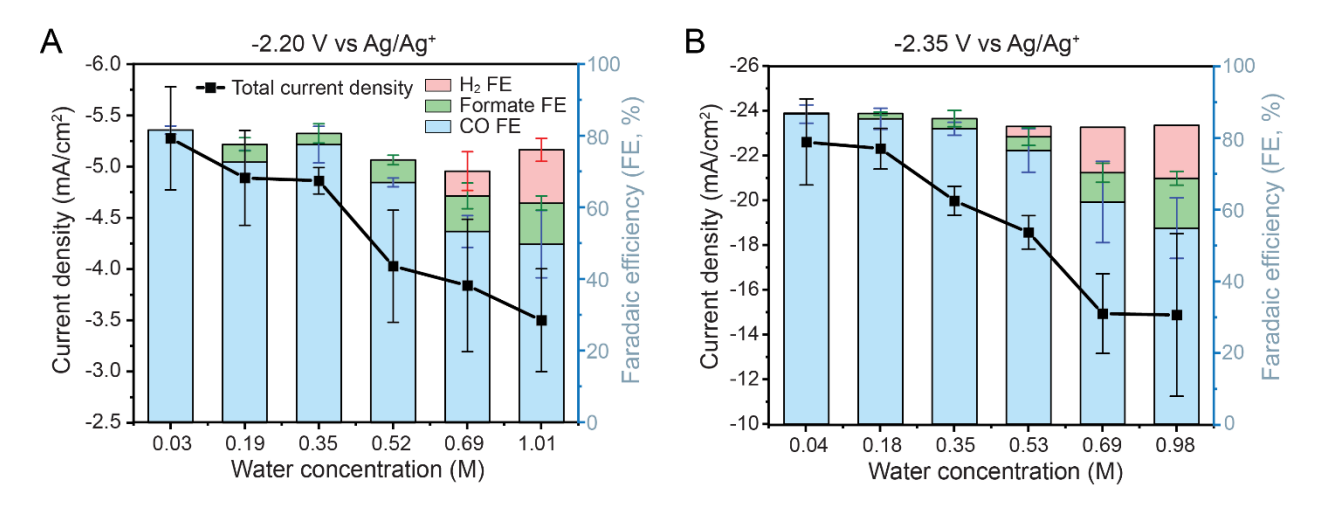


Figure 3. Steady-state CO₂ reduction in 0.7 M [EMIm][BF₄]-acetonitrile electrolytes doped with different concentrations of water. (A) Average total current density (line, left axis) and CO faradaic efficiency (bars, right axis) at -2.20 V vs Ag/Ag⁺. (B) Average total current density and CO faradaic efficiency at -2.35 V vs Ag/Ag⁺. At both applied potentials, the overall current density decreases with increasing water concentration, indicating that the participation of water-assisted CO₂ reduction compromises the activity of electrolytes.

We confirmed the formation and accumulation of [OH]⁻ in electrolytes by proton/deuterium (H/D) exchange of [EMIm]⁺ in an electrolyte with 0.7 M [EMIm][BF₄] and 0.6 M D₂O during electrolysis. The preparation of [D-EMIm][BF₄] demonstrated that nucleophiles including [OH]⁻ can interact with the C2-H of [EMIm]⁺ and facilitate proton exchange, validating the H/D exchange of [EMIm]⁺ as a qualitative probe of [OH]⁻. The extent of exchange was quantified by the decrease of C2-H integral in ¹H NMR spectra (Fig. S9). We found that under Ar-purged conditions, [EMIm]⁺ remained almost intact over 60 minutes with an applied potential up to -2.20 V vs Ag/Ag⁺. In contrast, rapid deuteration of [EMIm]⁺ occurred under CO₂-saturated condition starting from -2.05 V vs Ag/Ag⁺, and the rate of exchange increased at more cathodic applied potentials.

Nonetheless, the amount of deuterated [EMIm]⁺ (around 1.1×10^{-3} mol) was two orders higher than the number of electrons (around 1.4×10^{-5} mol) transferred across the electrode surface, meaning that the H/D exchange was not a potential-driven process (Fig. S9). Instead, the excessive H/D exchange was an indication of the formation of a [OH]⁻-rich local environment, confirming the active interaction of [OH]⁻ with [EMIm]⁺ when water-mediated CO₂ reduction becomes noticeable.

Conjugate bases impact the strength of electric field at interfaces.

Our group has previously explored how the extent of reorientation can act as a qualitative indicator of the strength of local electric field. ⁴⁵ To further understand how the accumulation of [OH]⁻ is related to the

drop in CO₂ reduction reactivity and CO selectivity, we collected *in situ* electrochemical surface-enhanced Raman scattering (SERS) spectra on an electrochemically roughened pc-Ag electrode in 0.7 M [EMIm][BF₄]-acetonitrile electrolytes with different water concentrations. Figure 4 shows the potential-dependent spectral change in the ring deformation region (1200 to 1700 cm⁻¹) of [EMIm]⁺ in CO₂-saturated electrolytes with water concentrations of 0.02 M, 0.40 M, and 1.11 M.

In the electrolyte with 0.02 M water, a peak at 1344 cm⁻¹ appeared and rapidly grew when the applied potential was decreased from open-circuit potential (-0.7 V vs Ag/Ag⁺) to -2.5 V vs Ag/Ag⁺. Meanwhile, a slightly weaker peak at 1561 cm⁻¹ emerged and the peak at 1417 cm⁻¹ diminished when the applied potential became more negative than -1.5 V vs Ag/Ag⁺. Eventually, only three main peaks at 1561 cm⁻¹, 1377 cm⁻¹, and 1344 cm⁻¹ were observed at -2.5 V vs Ag/Ag⁺. Since similar spectral changes in peaks at 1561 cm⁻¹, 1417 cm⁻¹, and 1344 cm⁻¹ were observed in the same electrolyte purged by Ar (Fig. S10), we interpret these changes as results of the collective reorientation of [EMIm]⁺ driven by electric fields at electrode-electrolyte interface. ⁵⁹⁻⁶³

The peak at 1417 cm⁻¹ was assigned to in-plane antisymmetric stretching of the imidazolium ring. ^{60,64,65} A comparison with *in situ* electrochemical SERS of 0.7 M [D-EMIm][BF₄] deuteration (Fig. S11) shows that at open-circuit potential, besides the red shift of C2-H stretching from over 3000 cm⁻¹ to 2329 cm⁻¹, the peak at 1417 cm⁻¹ exhibits the most pronounced red shift of 14 cm⁻¹ after the deuteration of C2-H, which further indicates the origination of the 1417 cm⁻¹ peak from an in-plane ring stretching mode involving C2. In contrast, none of three peaks at 1561 cm⁻¹, 1417 cm⁻¹, and 1344 cm⁻¹ observed at negative applied potentials shows red shift after the deuteration of C2-H, which indicates that none of them corresponds to in-plane stretching modes involving C2. Since all in-plane stretching modes from the same planar aromatic molecule are expected to be enhanced or suppressed in a similar manner in SERS, ⁶⁶ the absence of a peak corresponding to C2-related in-plane stretching also suggests that none of the three peaks originates from in-plane stretching modes of imidazolium ring.

SERS only enhances vibration modes with polarizability tensors perpendicular to metal surfaces based on surface selection rules. ^{66,67} Therefore, the disappearance of the peak at 1417 cm⁻¹ and 2329 cm⁻¹ (Fig. S12), together with the irrelevance of peaks at 1561 cm⁻¹, 1417 cm⁻¹, and 1344 cm⁻¹ to in-plane stretching in 0.7 M [D-EMIm][BF₄] at negative applied potentials, confirm that [EMIm]⁺ collectively reorients in such a way that the imidazolium rings become parallel to the electrode surface in response to the interfacial electric field. Further, the constant spectral features of electrolytes with 0.02 M water over a wide range of applied potentials reflected that the strong electric field at electrode-electrolyte interface is maintained during CO₂ reduction.

Electrolytes with 0.40 M and 1.11 M water exhibited spectral changes similar to the electrolyte with 0.02 M water when the applied potential was swept from open-circuit potential to -2.1 V vs Ag/Ag⁺ (Fig. 4B). However, the peak at 1417 cm⁻¹ recovered back to the open-circuit relative intensity when the applied potential was further decreased to -2.3 V vs Ag/Ag⁺, indicating the loss of electric field-driven collective reorientation of [EMIm]⁺. Notably, the recovery of the peak at 1417 cm⁻¹ only occurred under CO₂-saturated conditions but not Ar-purged conditions (Fig. S13), meaning that the disruption of [EMIm]⁺ reorientation was closely related to the participation of water-mediated CO₂ reduction.

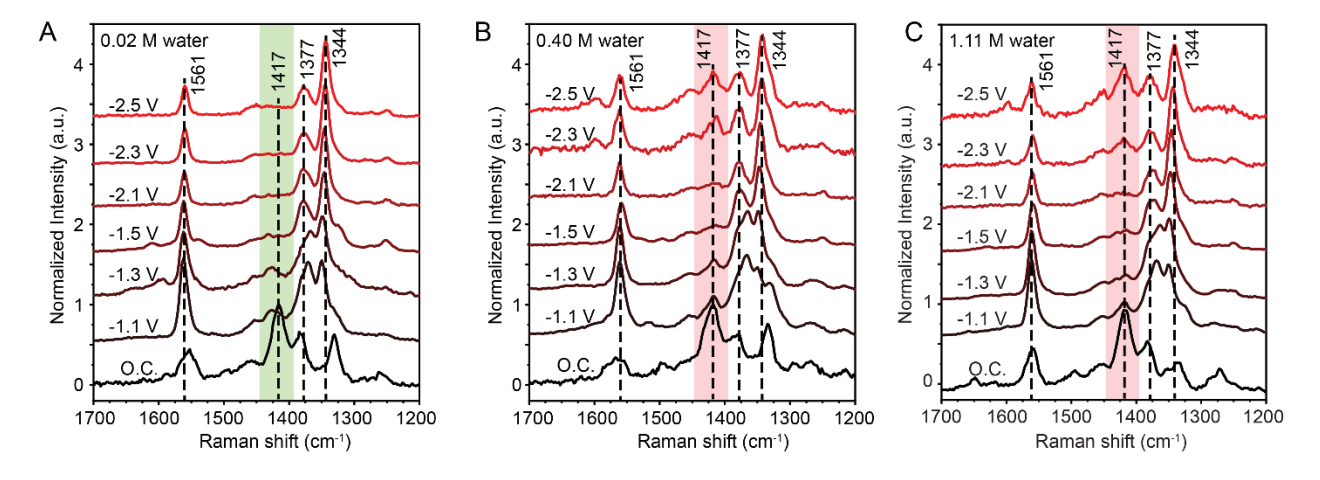


Figure 4. *In situ* surface-enhanced Raman spectroscopy of CO₂-saturated 0.7 M [EMIm][BF₄]-acetonitrile electrolyte doped with (A) 0.02 M, (B) 0.40 M, and (C) 1.11 M water in the ring deformation range on a polycrystalline-Ag electrode. In (A), the relative peak intensity at 1344 cm⁻¹ increases and the peak at 1417 cm⁻¹ decreases (green shading) when applied potential sweeps to cathodic direction, indicating the collective reorientation of [EMIm]⁺ at electrode-electrolyte interface. In (B) and (C), the peak at 1417 cm⁻¹ recovers (red shading) when the applied potential was decreased below -2.1 V, indicating the interruption of the collective reorientation of [EMIm]⁺ likely due to the generation of anionic [OH]⁻ co-ions.

We interpret that the loss of collective reorientation of [EMIm]⁺ in electrolytes with higher water concentrations results from the weakening of electric fields at electrode-electrolyte interface. Recent findings in surface force community show that correlations between cations and anions occur in concentrated ionic liquid electrolytes, which reduces the net density of "free" ions available to participate in screening. ^{30,32,68-71} As a result, concentrated ionic liquid electrolytes exhibit larger screening lengths of charged surfaces and thus a lower interfacial electric field. Our prior study demonstrated that the weakened electric field in concentrated [EMIm][BF₄]-acetonitrile electrolytes resulted in lower reactivity in CO₂ reduction.

H/D exchange results (Fig. S9) suggest that anionic co-ion [OH]⁻ are formed and accumulated on the cathode when water acts as the proton donor for CO₂ reduction. The buildup of [OH]⁻ (or [HCO₃]⁻ after

combining with CO₂) within the electric double layer due to ongoing electrolysis leads to a scenario analogous to concentrated ionic liquid electrolytes, where negative charges associated with these anionic co-ions counteract the surface potential of the electrode and weaken the electric field immediately adjacent to the electrode surface. Such a weaker electric field is less effective in stabilizing the key intermediate CO₂. formed during CO₂ reduction, resulting in a lower reaction rate (Fig. 5A). In contrast, when [EMIm]⁺ is acting as the proton donor, the formation of carbene and subsequent [EMIm-COO] adducts avoids the accumulation of anionic co-ions, maintaining the strong electric field at interface (Fig. 5B).

The weaker interfacial electric field when water acts as the primary proton donor could also account for the increased selectivity of formate and H₂ during prolonged electrolysis. CO₂ reduction pathways leading to CO and formate have been proposed to proceed via CO₂. intermediates that adsorb on a surface through C atom (*COO.) and O atom (*OCO.), respectively. 72,73 We postulate that the higher electronegativity of oxygen compared with carbon suggests that *COO. possesses a dipole that can be better stabilized by interfacial electric fields on a cathode, leading to selective CO production when a strong electric field exists. In contrast, when the interfacial electric field is weakened by accumulation of anionic co-ions, stabilization of *COO. will be less pronounced compared to *OCO. with an inverted dipole and adsorbed hydrogen (*H) that is nonpolar, causing a decrease in the selectivity toward CO and an increase in formate and H₂.

In addition, the loss of collective reorientation of [EMIm]⁺ may also contribute to decreasing CO₂ reduction rates. [EMIm]⁺ parallel to the electrode surface could be an orientation necessary for efficient transfer of C2-H to CO₂. Previous kinetic studies indicated that [EMIm]⁺ still participates in proton donation during CO₂ reduction through mixed mechanisms even when water concentrations exceeded 1.11 M. As a result, the loss of parallelly reoriented [EMIm]⁺ in a weaker electric field caused by [OH]⁻ or [HCO₃]⁻ accumulation would decrease the availability of protons from [EMIm]⁺, further decreasing the rate of CO₂ reduction.

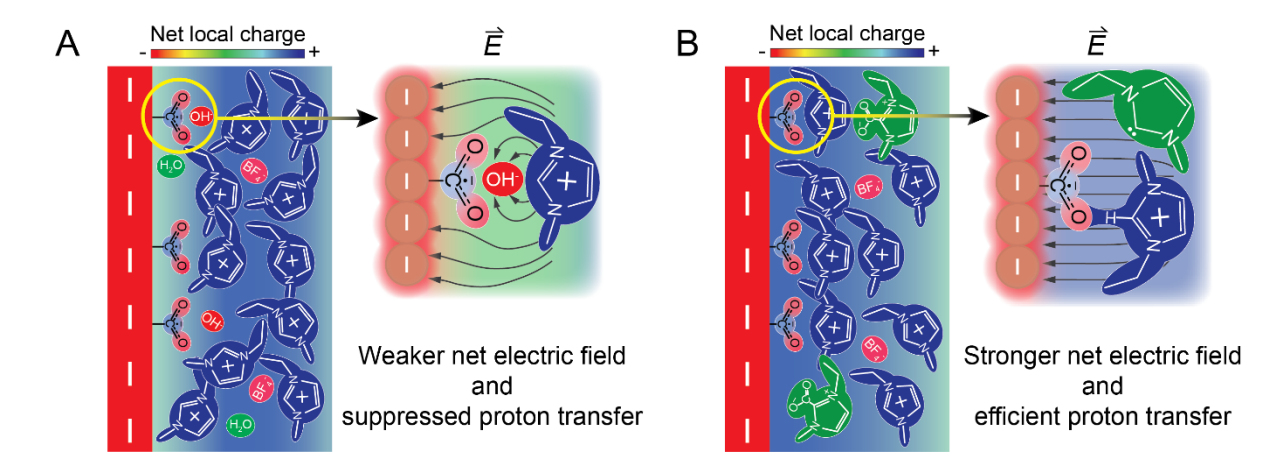


Figure 5. Schematics showing how the charge of proton donors and their conjugate bases influence steady-state CO_2 reduction activity in $[EMIm][BF_4]$ -acetonitrile electrolytes by modifying local microenvironment. (A) Microenvironment with neutral proton donors. Neutral proton donors, such as water, compromise long-term reaction activity by releasing negative co-ions, which not only weaken local electric field (\vec{E} , represented by sparser field lines) but also suppress interactions between CO_2 with other proton donors such as $[EMIm]^+$. (B) Microenvironment with cationic proton donors. In contrast, cationic proton donors release neutral conjugate bases that help maintain a higher local electric field (represented by denser field lines) and maintain interactions between CO_2 and unreacted $[EMIm]^+$, leading to higher long-term reaction activity. To more clearly show the structure of $[EMIm]^+$ and its interaction with CO_2 , $[EMIm]^+$ is not drawn in parallel to the electrode surface in this schematic.

Maintaining steady-state reactivity by sourcing protons from positive donors and releasing neutral conjugate bases.

Taken together, sourcing protons from [EMIm]⁺ in CO₂ reduction releases carbene as the conjugate base, and this carbene is then converted to zwitterionic [EMIm-CO₂] adduct, which neither compromises the electric field at electron-electrolyte interface nor interferes with proton donation from other [EMIm]⁺. Together, these factors are key for enabling high and stable CO₂ reduction reactivity needed to prolong CO₂ reduction electrolysis operated at high current densities.

To further evaluate how the relative charge state of proton donors and conjugate bases influences the performance of electrolytes for CO₂ reduction, we conducted CO₂ reduction in 0.7 M [EMMIm][BF₄]-acetonitrile electrolytes at -2.5 V vs Ag/Ag⁺ with 0.1 M different proton donors, namely water and triethylamine hydrochloride ([Et₃NH][Cl]), which releases negative [OH]⁻ (or [HCO₃]⁻ after conversion) and neutral [Et₃N] as conjugate bases, respectively. With water as the proton donor, the total current density rapidly dropped from over -100 mA/cm² to about -2 mA/cm² within a minute (Fig. S14), similar to the reported decreased reactivity of 0.5 M [EMMIm][BF₄]-acetonitrile electrolytes and was attributed to the formation of [EMMIm][HCO₃] due to co-ion generation. In contrast, when [Et₃NH]⁺ was used as the proton donor, the current density toward CO₂ reduction was maintained at around -40 mA/cm² for over one hour (Fig. S14), confirming that sourcing protons from positive donors and releasing neutral conjugate bases were crucial for a better performance of electrolytes during long-term CO₂ reduction.

Our results highlight that in addition to the intrinsic kinetics, the electrostatic influence of conjugate bases and proton donors play critical roles in determining the performance of CO₂ reduction in non-aqueous electrolytes. Sourcing protons from positively charged proton donors such as [EMIm]⁺ and [Et₃NH]⁺ leads to the formation of neutral conjugate bases that do not compromise local potential gradients needed to drive CO₂ electrochemical conversion. In contrast, neutral proton donors such as water release negatively charged

conjugate bases, which suppress the activity of electrolytes through both weakening local potential gradients and generation of non-reactive [HCO₃] complexes.

Conclusion

In this study, we demonstrated that [EMIm]⁺ can directly participate in the CO₂ electroreduction by donating C2-H to CO₂. The donation of C2-H converts [EMIm]⁺ to carbenes that rapidly coordinate to dissolved CO₂ to form [EMIm-CO₂] adducts. A comparison between CO₂ reduction using [EMIm]⁺ or water as the proton donor indicates that the formation of [EMIm-CO₂] adducts is essential in maintaining the activity and stability of the electrolyte over steady-state electrolysis. Although [EMIm-CO₂] does not directly participate in CO₂ reduction, the charge-neutral nature of the zwitterionic complex prevents electrogenerated conjugate bases from weakening the electric field near an electrode surface and coordinating with unreacted [EMIm]⁺. In conclusion, our work highlights how the chemical and ionic properties of local microenvironment at electrode-electrolyte interface are controlled by reactants, products, and all side products collectively during CO₂ electrochemical conversion. More broadly, our determination that electrogeneration of co-ionic species substantially weakens electrochemical driving forces by lowering local potential gradients should be a generally applicable mechanism with high relevance to other reactions, such as water splitting and nitrate electroreduction. ⁷⁴⁻⁷⁶

Experimental Details

Chemicals. 1-Ethyl-3-methylimidazolium tetrafluoroborate ([EMIm][BF₄], >98% purity, Sigma-Aldrich) and 1-ethyl-2,3-dimethylimidazolium tetrafluoroborate ([EMMIm][BF₄], >98% purity, Iolitec) were used as purchased without further purification. Deuterated [EMIm][BF₄] ([D-EMIm][BF₄]) was prepared by stirring 10 mL (0.065 mol) of [EMIm][BF₄] in 80 mL D₂O with pD tuned to 8 using 1 M NaOD (prepared from NaOD 40 wt% in D₂O, Sigma-Aldrich) for 8 hours at room temperature. After stirring, the solution was neutralized by 37% HCl. D₂O (and trace amount of H₂O) of the neutralized solution and extra HCl was first removed by a rotary evaporator (BUCHI Rotavapor R-300), and then more thoroughly dried by a vacuum drying oven (Yamato ADP200C) at 60 °C for two days. The crude [D-EMIm][BF₄] was then washed and filtered using acetone to remove insoluble side product NaCl. Acetone was then removed from washed and filtered [D-EMIm][BF₄] using a rotary evaporator and a vacuum drying oven. Tetrabutylammonium tetrafluoroborate ([TBA][BF₄], >99% purity, TCI) was purified by activated charcoal (Sigma-Aldrich) to remove halide impurities before use. HPLC grade acetonitrile and methanol were purchased from Fisher Chemicals. Deuterium oxide (D₂O) and triethylamine hydrochloride ([Et₃NH][CI], 101 at%) were from Sigma-Aldrich. Potassium bromide was from MP Biomedicals. Silver nitrate (99.9+%

metal basis) was from Alfa Aesar. Deuterated acetonitrile (>98.5% atom D) was from Acros Organics. Ultrapure water (Milli-Q, \geq 18.2 M Ω cm) was used in all experiments.

Electrochemical Methods. A BioLogic VSP potentiostat was used for electrochemical measurements. A polycrystalline Ag (pc-Ag) electrode (BASi) was used as the working electrode in all experiments. All current densities reported were normalized to the geometric area of the pc-Ag electrode (0.071 cm²). Before every experiment, the pc-Ag electrode was polished to a mirror finish based on established protocols using 15 μm, 3 μm, and 1 μm diamond polish and then 0.05 μm alumina (BASi), followed by ultrasonication in water. An Ag/Ag⁺ non-aqueous reference electrode was used in all experiments, and the filling solution was an acetonitrile solution of 0.1 M [TBA][BF₄] and 0.01 M AgNO₃. The counter electrode was a coiled platinum wire. CV measurements were performed in a homemade one-compartment electrochemical cell at a scan rate of 50 mV/s. LSV (scan rate 50 mV/s), and CA and measurements were conducted in a twocompartment H-cell. A Nafion 117 membrane was used in H-cell for transporting cations between analyte and catholyte. The Nafion 117 membranes were activated following previously reported methods and stored in 0.1 M [TBA][BF₄]-acetonitrile solutions when not being used. Electrolytes were purged by targeting gas (Ar or CO₂ as stated) for 15 minutes at 9.2 sccm before all experiments, and the gas purging was kept during CA measurements. In CA measurements, the potentials were held at designated values for 190 min if not otherwise stated, and the electrolyte was stirred at 600 rpm throughout experiments. To compare activities of 0.7 M [D-EMIm][BF₄] and [EMIm][BF₄]-acetonitrile electrolytes, [EMIm][BF₄] was treated by same procedures used to produce [D-EMIm][BF₄] (see Chemicals section) but using regular water (H₂O) and NaOH in order to eliminate the impact on activity brought by treatment alone.

Product Analysis. Gas products from CA experiments were analyzed by an online gas chromatograph (GC, SRI Multiple Gas Analyzer #5) equipped with a thermal conductivity detector (TCD) and a flame-ionization detector (FID) coupled with a methanizer. The TCD detector was connected to a HayeSep D column, and the FID was connected to a HayeSep D and a Molesieve 5A column (Restek) in sequence. Ultrahigh purity grade He (Airgas) was used as the carrier gas. For 190 min CA measurements, components of outlet gas mixtures were analyzed by GC every 23 minutes starting from 6 minute, and the corresponding faradaic efficiency was calculated using the equation:

$$FE(\%) = \frac{\frac{v}{60S/min} \times \frac{y}{24,000cm^3/mol} \times N \times F}{i} \times 100\%$$

where v = 9.2 standard cubic centimeters per minute (sccm) is the flow rate of CO₂, y is the concentration of product measured from GC in the unit of mole (volume) fraction, N = 2 is the number of electrons consumed to generate one CO molecule from one CO₂ molecule, F = 96500 C mol⁻¹ is the Faraday constant, and *i* is the total current passing through the working electrode in the unit of ampere. Steady-state CA results

were obtained by averaging current densities and faradaic efficiencies after 30 minutes of holding potentials, and the standard deviations are used as error bars after being adjusted by instrumental errors. For Tafel analysis, the flow rate (v) was set to 5 sccm, and average current densities and faradaic efficiencies over the initial 4 minutes of holding potentials were used. Standard deviations of current densities over the 4 minutes are used to generate error bars. Fresh electrolytes and freshly polished pc-Ag electrodes were used to collect each data point in Tafel analysis to minimize the influence of side product buildup in electrolyte and on electrode surface. Liquid products generated during CA experiments were analyzed using a 400 MHz NMR spectrometer (Bruker Avance) with a BBFO probe. The electrolytes were mixed with deuterated acetonitrile in 1:1 ratio to prepare an NMR sample. The amount of [EMIm-COO] adduct was estimated based on the ratio between integrals of C4/C5-Hs on adduct and unreacted [EMIm]⁺ in ¹H NMR. The amount and faradaic efficiency of formate was estimated based on the ratio between the integral of formate peak at around 8.65 ppm and the sum of integrals of C4/C5-Hs for both adduct and unreacted [EMIm]⁺. The average and standard deviation from three CA replicates were used to obtain average faradaic efficiency and error bars of formate formation. Water concentrations of fresh or reacted electrolytes were measured using a Coulometric Karl Fisher Tritrator (Mettler Toledo C10S).

SERS Measurements. In situ electrochemical surface-enhanced Raman scattering (SERS) measurements were carried out using a single-compartment PTFE electrochemical cell with an L-shape pc-Ag working electrode (Shanghai Fanyue Electronic Technology Co. Ltd). The L-shape pc-Ag electrode was made SERS active by electrochemically roughening following reported method in literature with modifications. 77 In brief, a polished L-shape pc-Ag electrode was cycled between -0.42 V and +0.28V versus open-circuit potential (OCP) in 0.1 M potassium bromide aqueous solution for three cycles under Ar purging. The electrode was held at -0.42 V vs OCP for 10 seconds at the end of cycling to desorb bromide from silver surface as much as possible, and the electrode was vigorously rinsed with water immediately after the roughening to remove chemical and silver oxide residues. Scanning electron microscope (SEM, Zeiss GeminiSEM 450) confirmed the nanostructured surface of the L-shape pc-Ag electrode after roughening (Fig. S15). The counter electrode for in situ SERS was a coiled Pt wire, while the reference electrode was a non-aqueous Ag/Ag⁺ (0.01 M AgNO₃) electrode. Electrolytes were purged with either Ar or CO₂ for 20 minutes at 20 sccm prior to all measurements. SERS spectra were collected using a Thermo-Fisher Scientific DXRxi Raman Imaging Microscope with a 532 nm excitation laser and a 10x objective. The laser power was 8.0 mW, the acquisition time was 0.033 s (30 Hz), and 100 scans were collected for each spectrum. The potential was swept from -0.9 V to -2.5 V vs Ag/Ag⁺ at a step of 0.2 V to collect SERS spectra at different applied potentials.

AUTHOR INFORMATION

Corresponding Author

* Email: gebbie@wisc.edu

Author Contributions

The manuscript was written through contributions of all authors. All authors have given approval to the final version of the manuscript.

Notes

The authors declare no competing financial interest.

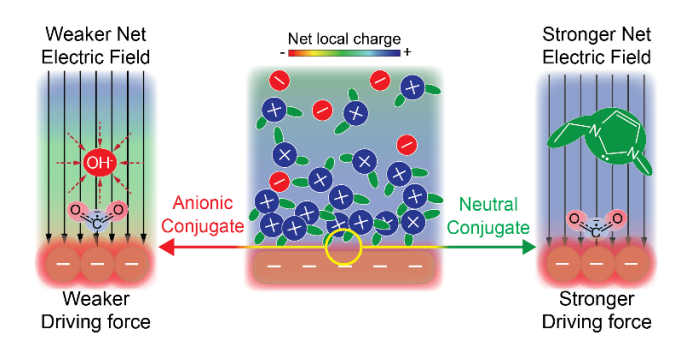
ASSOCIATED CONTENT

Supporting Information. Additional experimental data. This material is available free of charge via the Internet at http://pubs.acs.org.

ACKNOWLEDGEMENT

This material is based upon work supported by the National Science Foundation under Award No. 2237311. M. A. G. acknowledges support from the Michael F. and Virginia H. Conway Assistant Professorship. B. L. acknowledges support from the Fenton-May Graduate Fellowship. The authors gratefully acknowledge use of facilities and instrumentation at the UW-Madison Wisconsin Centers for Nanoscale Technology (went.wisc.edu) partially supported by the NSF through the University of Wisconsin Materials Research Science and Engineering Center (DMR-1720415). The Bruker AVANCE 400 NMR spectrometer was supported by NSF grant CHE-1048642.

Table of Content Artwork



REFERENCES

- (1) Deng, B.; Huang, M.; Zhao, X.; Mou, S.; Dong, F., Interfacial Electrolyte Effects on Electrocatalytic CO2 Reduction. *ACS Catalysis* **2021**, *12* (1), 331-362. doi: 10.1021/acscatal.1c03501
- (2) Koolen, C. D.; Luo, W.; Züttel, A., From Single Crystal to Single Atom Catalysts: Structural Factors Influencing the Performance of Metal Catalysts for CO2 Electroreduction. *ACS Catalysis* **2022**, *13* (2), 948-973. doi: 10.1021/acscatal.2c03842
- (3) Nam, D. H.; De Luna, P.; Rosas-Hernandez, A.; Thevenon, A.; Li, F.; Agapie, T.; Peters, J. C.; Shekhah, O.; Eddaoudi, M.; Sargent, E. H., Molecular enhancement of heterogeneous CO(2) reduction. *Nature Materials* **2020**, *19* (3), 266-276. doi: 10.1038/s41563-020-0610-2
- (4) Wagner, A.; Sahm, C. D.; Reisner, E., Towards molecular understanding of local chemical environment effects in electro- and photocatalytic CO2 reduction. *Nature Catalysis* **2020**, *3* (10), 775-786. doi: 10.1038/s41929-020-00512-x
- (5) Xie, Y.; Ou, P.; Wang, X.; Xu, Z.; Li, Y. C.; Wang, Z.; Huang, J. E.; Wicks, J.; McCallum, C.; Wang, N.; Wang, Y.; Chen, T.; Lo, B. T. W.; Sinton, D.; Yu, J. C.; Wang, Y.; Sargent, E. H., High carbon utilization in CO2 reduction to multi-carbon products in acidic media. *Nature Catalysis* **2022**, *5* (6), 564-570. doi: 10.1038/s41929-022-00788-1
- (6) Gurkan, B.; Su, X.; Klemm, A.; Kim, Y.; Mallikarjun Sharada, S.; Rodriguez-Katakura, A.; Kron, K. J., Perspective and challenges in electrochemical approaches for reactive CO2 separations. *iScience* **2021**, *24* (12), 103422. doi: https://doi.org/10.1016/j.isci.2021.103422
- (7) Resasco, J.; Bell, A. T., Electrocatalytic CO2 Reduction to Fuels: Progress and Opportunities. *Trends in Chemistry* **2020**, *2* (9), 825-836. doi: https://doi.org/10.1016/j.trechm.2020.06.007
- (8) Marcandalli, G.; Monteiro, M. C. O.; Goyal, A.; Koper, M. T. M., Electrolyte Effects on CO(2) Electrochemical Reduction to CO. *Acc Chem Res* **2022**, *55* (14), 1900-1911. doi: 10.1021/acs.accounts.2c00080
- (9) Xu, A.; Govindarajan, N.; Kastlunger, G.; Vijay, S.; Chan, K., Theories for Electrolyte Effects in CO(2) Electroreduction. *Acc Chem Res* **2022**, *55* (4), 495-503. doi: 10.1021/acs.accounts.1c00679
- (10) Marcandalli, G.; Goyal, A.; Koper, M. T. M., Electrolyte Effects on the Faradaic Efficiency of CO(2) Reduction to CO on a Gold Electrode. *ACS Catal* **2021**, *11* (9), 4936-4945. doi: 10.1021/acscatal.1c00272
- (11) Monteiro, M. C. O.; Goyal, A.; Moerland, P.; Koper, M. T. M., Understanding Cation Trends for Hydrogen Evolution on Platinum and Gold Electrodes in Alkaline Media. *ACS Catal* **2021**, *11* (23), 14328-14335. doi: 10.1021/acscatal.1c04268
- (12) Goyal, A.; Koper, M. T. M., The Interrelated Effect of Cations and Electrolyte pH on the Hydrogen Evolution Reaction on Gold Electrodes in Alkaline Media. *Angew Chem Int Ed Engl* **2021**, *60* (24), 13452-13462. doi: 10.1002/anie.202102803
- (13) Goyal, A.; Koper, M. T. M., Understanding the role of mass transport in tuning the hydrogen evolution kinetics on gold in alkaline media. *J Chem Phys* **2021**, *155* (13), 134705. doi: 10.1063/5.0064330
- (14) Deng, W.; Zhang, P.; Seger, B.; Gong, J., Unraveling the rate-limiting step of two-electron transfer electrochemical reduction of carbon dioxide. *Nature Communications* **2022**, *13* (1), 803. doi: 10.1038/s41467-022-28436-z
- (15) Gu, J.; Liu, S.; Ni, W.; Ren, W.; Haussener, S.; Hu, X., Modulating electric field distribution by alkali cations for CO2 electroreduction in strongly acidic medium. *Nature Catalysis* **2022**, *5* (4), 268-276. doi: 10.1038/s41929-022-00761-y
- (16) Goyal, A.; Marcandalli, G.; Mints, V. A.; Koper, M. T. M., Competition between CO(2) Reduction and Hydrogen Evolution on a Gold Electrode under Well-Defined Mass Transport Conditions. *Journal of the American Chemical Society* **2020**, *142* (9), 4154-4161. doi: 10.1021/jacs.9b10061
- (17) Lu, X. K.; Lu, B.; Li, H.; Lim, K.; Seitz, L. C., Stabilization of Undercoordinated Cu Sites in Strontium Copper Oxides for Enhanced Formation of C2+ Products in Electrochemical CO2 Reduction. *ACS Catalysis* **2022**, *12* (11), 6663-6671. doi: 10.1021/acscatal.2c01019
- (18) Chu, A. T.; Surendranath, Y., Aprotic Solvent Exposes an Altered Mechanism for Copper-Catalyzed Ethylene Electrosynthesis. *Journal of the American Chemical Society* **2022**, *144* (12), 5359-5365. doi: 10.1021/jacs.1c12595
- (19) Figueiredo, M. C.; Ledezma-Yanez, I.; Koper, M. T. M., In Situ Spectroscopic Study of CO2 Electroreduction at Copper Electrodes in Acetonitrile. *ACS Catalysis* **2016**, *6* (4), 2382-2392. doi: 10.1021/acscatal.5b02543
- (20) Gomes, R. J.; Birch, C.; Cencer, M. M.; Li, C.; Son, S.-B.; Bloom, I. D.; Assary, R. S.; Amanchukwu, C. V., Probing Electrolyte Influence on CO2 Reduction in Aprotic Solvents. *The Journal of Physical Chemistry C* **2022**, 126 (32), 13595-13606. doi: 10.1021/acs.jpcc.2c03321

- (21) Joshi, P. B.; Karki, N.; Wilson, A. J., Electrocatalytic CO2 Reduction in Acetonitrile Enhanced by the Local Environment and Mass Transport of H2O. *ACS Energy Letters* **2022**, 7 (2), 602-609. doi: 10.1021/acsenergylett.1c02667
- (22) Matsubara, Y.; Grills, D. C.; Kuwahara, Y., Thermodynamic Aspects of Electrocatalytic CO2 Reduction in Acetonitrile and with an Ionic Liquid as Solvent or Electrolyte. *ACS Catalysis* **2015**, *5* (11), 6440-6452. doi: 10.1021/acscatal.5b00656
- Vasilyev, D. V.; Dyson, P. J., The Role of Organic Promoters in the Electroreduction of Carbon Dioxide. *ACS Catalysis* **2021**, *11* (3), 1392-1405. doi: 10.1021/acscatal.0c04283
- (24) Lau, G. P.; Schreier, M.; Vasilyev, D.; Scopelliti, R.; Gratzel, M.; Dyson, P. J., New Insights Into the Role of Imidazolium-Based Promoters for the Electroreduction of CO2 on a Silver Electrode. *Journal of the American Chemical Society* **2016**, *138* (25), 7820-7823. doi: 10.1021/jacs.6b03366
- (25) Motobayashi, K.; Maeno, Y.; Ikeda, K., In Situ Spectroscopic Characterization of an Intermediate of CO2 Electroreduction on a Au Electrode in Room-Temperature Ionic Liquids. *The Journal of Physical Chemistry C* **2022**, 126 (29), 11981-11986. doi: 10.1021/acs.jpcc.2c03012
- Rosen, B. A.; Salehi-Khojin, A.; Thorson, M. R.; Zhu, W.; Whipple, D. T.; Kenis, P. J. A.; Masel, R. I., Ionic Liquid–Mediated Selective Conversion of CO2 to CO at Low Overpotentials. *Science* **2011**, *334* (6056), 643-644. doi: 10.1126/science.1209786
- (27) Vasilyev, D. V.; Shyshkanov, S.; Shirzadi, E.; Katsyuba, S. A.; Nazeeruddin, M. K.; Dyson, P. J., Principal Descriptors of Ionic Liquid Co-catalysts for the Electrochemical Reduction of CO2. *ACS Applied Energy Materials* **2020**, *3* (5), 4690-4698. doi: 10.1021/acsaem.0c00330
- Wang, Y.; Hatakeyama, M.; Ogata, K.; Wakabayashi, M.; Jin, F.; Nakamura, S., Activation of CO2 by ionic liquid EMIM-BF4 in the electrochemical system: a theoretical study. *Physical Chemistry Chemical Physics* **2015**, *17* (36), 23521-23531. doi: 10.1039/c5cp02008e
- (29) García Rey, N.; Dlott, D. D., Structural Transition in an Ionic Liquid Controls CO2 Electrochemical Reduction. *The Journal of Physical Chemistry C* **2015**, *119* (36), 20892-20899. doi: 10.1021/acs.jpcc.5b03397
- (30) Gebbie, M. A.; Smith, A. M.; Dobbs, H. A.; Lee, A. A.; Warr, G. G.; Banquy, X.; Valtiner, M.; Rutland, M. W.; Israelachvili, J. N.; Perkin, S.; Atkin, R., Long range electrostatic forces in ionic liquids. *Chemical Communications* **2017**, *53* (7), 1214-1224. doi: 10.1039/c6cc08820a
- (31) Hayes, R.; Warr, G. G.; Atkin, R., Structure and nanostructure in ionic liquids. *Chemical Reviews* **2015**, *115* (13), 6357-6426. doi: 10.1021/cr500411q
- (32) Gebbie, M. A.; Dobbs, H. A.; Valtiner, M.; Israelachvili, J. N., Long-range electrostatic screening in ionic liquids. *Proceedings of the National Academy of Sciences of the United States of America* **2015**, *112* (24), 7432-7437. doi: 10.1073/pnas.1508366112
- (33) Voegtle, M. J.; Pal, T.; Pennathur, A. K.; Menachekanian, S.; Patrow, J. G.; Sarkar, S.; Cui, Q.; Dawlaty, J. M., Interfacial Polarization and Ionic Structure at the Ionic Liquid–Metal Interface Studied by Vibrational Spectroscopy and Molecular Dynamics Simulations. *The Journal of Physical Chemistry B* **2021**, *125* (10), 2741-2753. doi: 10.1021/acs.jpcb.0c11232
- (34) Voskian, S.; Brown, P.; Halliday, C.; Rajczykowski, K.; Hatton, T. A., Amine-Based Ionic Liquid for CO2 Capture and Electrochemical or Thermal Regeneration. *ACS Sustainable Chemistry & Engineering* **2020**, *8* (22), 8356-8361. doi: 10.1021/acssuschemeng.0c02172
- (35) Mao, X.; Brown, P.; Červinka, C.; Hazell, G.; Li, H.; Ren, Y.; Chen, D.; Atkin, R.; Eastoe, J.; Grillo, I.; Padua, A. A. H.; Costa Gomes, M. F.; Hatton, T. A., Self-assembled nanostructures in ionic liquids facilitate charge storage at electrified interfaces. *Nature Materials* **2019**, *18* (12), 1350-1357. doi: 10.1038/s41563-019-0449-6
- (36) Chaban, V. V.; Voroshylova, I. V.; Kalugin, O. N.; Prezhdo, O. V., Acetonitrile boosts conductivity of imidazolium ionic liquids. *The Journal of Physical Chemistry B* **2012**, *116* (26), 7719-7727. doi: 10.1021/jp3034825
- (37) Stoppa, A.; Hunger, J.; Buchner, R., Conductivities of Binary Mixtures of Ionic Liquids with Polar Solvents. *Journal of Chemical & Engineering Data* **2009**, *54* (2), 472-479. doi: 10.1021/je800468h
- (38) Garcia Rey, N.; Dlott, D. D., Effects of water on low-overpotential CO(2) reduction in ionic liquid studied by sum-frequency generation spectroscopy. *Physical Chemistry Chemical Physics* **2017**, *19* (16), 10491-10501. doi: 10.1039/c7cp00118e
- (39) Kemna, A.; García Rey, N.; Braunschweig, B., Mechanistic Insights on CO2 Reduction Reactions at Platinum/[BMIM][BF4] Interfaces from In Operando Spectroscopy. *ACS Catalysis* **2019**, *9* (7), 6284-6292. doi: 10.1021/acscatal.9b01033

- (40) Neyrizi, S.; Kiewiet, J.; Hempenius, M. A.; Mul, G., What It Takes for Imidazolium Cations to Promote Electrochemical Reduction of CO(2). *ACS Energy Letters* **2022,** 7 (10), 3439-3446. doi: 10.1021/acsenergylett.2c01372
- (41) Ratschmeier, B.; Braunschweig, B., Cations of Ionic Liquid Electrolytes Can Act as a Promoter for CO2 Electrocatalysis through Reactive Intermediates and Electrostatic Stabilization. *The Journal of Physical Chemistry C* **2021**, *125* (30), 16498-16507. doi: 10.1021/acs.jpcc.1c02898
- (42) Ratschmeier, B.; Kemna, A.; Braunschweig, B., Role of H2O for CO2 Reduction Reactions at Platinum/Electrolyte Interfaces in Imidazolium Room-Temperature Ionic Liquids. *ChemElectroChem* **2020**, *7* (7), 1765-1774. doi: 10.1002/celc.202000316
- (43) Sharifi Golru, S.; Biddinger, E. J., Effect of anion in diluted imidazolium-based ionic liquid/buffer electrolytes for CO2 electroreduction on copper. *Electrochimica Acta* **2020**, *361* 136787. doi: https://doi.org/10.1016/j.electacta.2020.136787
- (44) Yang, J.; Kang, X.; Jiao, J.; Xing, X.; Yin, Y.; Jia, S.; Chu, M.; Han, S.; Xia, W.; Wu, H.; He, M.; Han, B., Ternary Ionic-Liquid-Based Electrolyte Enables Efficient Electro-reduction of CO2 over Bulk Metal Electrodes. *Journal of the American Chemical Society* **2023**, Ahead of Print, doi: 10.1021/jacs.3c03259
- Liu, B.; Guo, W.; Gebbie, M. A., Tuning Ionic Screening To Accelerate Electrochemical CO2 Reduction in Ionic Liquid Electrolytes. *ACS Catalysis* **2022**, *12* (15), 9706-9716. doi: 10.1021/acscatal.2c02154
- (46) Sassenburg, M.; Kelly, M.; Subramanian, S.; Smith, W. A.; Burdyny, T., Zero-Gap Electrochemical CO(2) Reduction Cells: Challenges and Operational Strategies for Prevention of Salt Precipitation. *ACS Energy Letters* **2023**, 8 (1), 321-331. doi: 10.1021/acsenergylett.2c01885
- (47) Kash, B. C.; Gomes, R. J.; Amanchukwu, C. V., Mitigating Electrode Inactivation during CO2 Electrocatalysis in Aprotic Solvents with Alkali Cations. *The Journal of Physical Chemistry Letters* **2023**, *14* (4), 920-926. doi: 10.1021/acs.jpclett.2c03498
- (48) Matsuki, Y.; Ohnishi, N.; Kakeno, Y.; Takemoto, S.; Ishii, T.; Nagao, K.; Ohniya, H., Aryl radical-mediated N-heterocyclic carbene catalysis. *Nature Communications* **2021**, *12* (1), 3848. doi: 10.1038/s41467-021-24144-2
- (49) Bellotti, P.; Koy, M.; Hopkinson, M. N.; Glorius, F., Recent advances in the chemistry and applications of N-heterocyclic carbenes. *Nature Reviews Chemistry* **2021**, *5* (10), 711-725. doi: 10.1038/s41570-021-00321-1
- (50) Michez, R.; Doneux, T.; Buess-Herman, C.; Luhmer, M., NMR Study of the Reductive Decomposition of [BMIm][NTf(2)] at Gold Electrodes and Indirect Electrochemical Conversion of CO(2). *Chemphyschem* **2017**, *18* (16), 2208-2216. doi: 10.1002/cphc.201700421
- Sun, L.; Ramesha, G. K.; Kamat, P. V.; Brennecke, J. F., Switching the reaction course of electrochemical CO(2) reduction with ionic liquids. *Langmuir* **2014**, *30* (21), 6302-6308. doi: 10.1021/la5009076
- (52) Dey, S.; Masero, F.; Brack, E.; Fontecave, M.; Mougel, V., Electrocatalytic metal hydride generation using CPET mediators. *Nature* **2022**, *607* (7919), 499-506. doi: 10.1038/s41586-022-04874-z
- (53) Shao, F.; Xia, Z.; You, F.; Wong, J. K.; Low, Q. H.; Xiao, H.; Yeo, B. S., Surface Water as an Initial Proton Source for the Electrochemical CO Reduction Reaction on Copper Surfaces. *Angewandte Chemie International Edition* **2023**, *62* (3), e202214210. doi: 10.1002/anie.202214210
- (54) Sarkar, S.; Maitra, A.; Lake, W. R.; Warburton, R. E.; Hammes-Schiffer, S.; Dawlaty, J. M., Mechanistic Insights about Electrochemical Proton-Coupled Electron Transfer Derived from a Vibrational Probe. *Journal of the American Chemical Society* **2021**, *143* (22), 8381-8390. doi: 10.1021/jacs.1c01977
- (55) Warburton, R. E.; Soudackov, A. V.; Hammes-Schiffer, S., Theoretical Modeling of Electrochemical Proton-Coupled Electron Transfer. *Chemical Reviews* **2022**, *122* (12), 10599-10650. doi: 10.1021/acs.chemrev.1c00929
- (56) Zhu, X.; Huang, J.; Eikerling, M., Electrochemical CO2 Reduction at Silver from a Local Perspective. *ACS Catalysis* **2021**, *11* (23), 14521-14532. doi: 10.1021/acscatal.1c04791
- (57) Jackson, M. N.; Surendranath, Y., Donor-Dependent Kinetics of Interfacial Proton-Coupled Electron Transfer. *Journal of the American Chemical Society* **2016**, *138* (9), 3228-3234. doi: 10.1021/jacs.6b00167
- (58) Rosen, J.; Hutchings, G. S.; Lu, Q.; Rivera, S.; Zhou, Y.; Vlachos, D. G.; Jiao, F., Mechanistic Insights into the Electrochemical Reduction of CO2 to CO on Nanostructured Ag Surfaces. *ACS Catalysis* **2015**, *5* (7), 4293-4299. doi: 10.1021/acscatal.5b00840
- (59) Santos, V. O.; Alves, M. B.; Carvalho, M. S.; Suarez, P. A. Z.; Rubim, J. C., Surface-Enhanced Raman Scattering at the Silver Electrode/Ionic Liquid (BMIPF6) Interface. *The Journal of Physical Chemistry B* **2006**, *110* (41), 20379-20385. doi: 10.1021/jp0643348
- (60) Santos, V. O.; Leite, I. R.; Brolo, A. G.; Rubim, J. C., The electrochemical reduction of CO2 on a copper electrode in 1-n-butyl-3-methyl imidazolium tetrafluoroborate (BMI.BF4) monitored by surface-enhanced Raman scattering (SERS). *Journal of Raman Spectroscopy* **2016**, *47* (6), 674-680. doi: 10.1002/jrs.4871

- (61) Yuan, Y.-X.; Niu, T.-C.; Xu, M.-M.; Yao, J.-L.; Gu, R.-A., Probing the adsorption of methylimidazole at ionic liquids/Cu electrode interface by surface-enhanced Raman scattering spectroscopy. *Journal of Raman Spectroscopy* **2009**, *41* (5), 516-523. doi: 10.1002/jrs.2480
- (62) Paschoal, V. H.; Faria, L. F. O.; Ribeiro, M. C. C., Vibrational Spectroscopy of Ionic Liquids. *Chemical Reviews* **2017**, *117* (10), 7053-7112. doi: 10.1021/acs.chemrev.6b00461
- (63) Fu, J. Y.; Li, X. C.; Yu, Z.; Huang-Fu, X. N.; Fan, J. A.; Zhang, Z. Q.; Huang, S.; Zheng, J. F.; Wang, Y. H.; Zhou, X. S., In Situ Raman Monitoring of Potential-Dependent Adlayer Structures on the Au(111)/Ionic Liquid Interface. *Langmuir* **2022**, *38* (19), 6209-6216. doi: 10.1021/acs.langmuir.2c00703
- (64) Heimer, N. E.; Del Sesto, R. E.; Meng, Z.; Wilkes, J. S.; Carper, W. R., Vibrational spectra of imidazolium tetrafluoroborate ionic liquids. *Journal of Molecular Liquids* **2006**, *124* (1-3), 84-95. doi: 10.1016/j.molliq.2005.08.004
- (65) Kiefer, J.; Fries, J.; Leipertz, A., Experimental Vibrational Study of Imidazolium-Based Ionic Liquids: Raman and Infrared Spectra of 1-Ethyl-3-methylimidazolium Bis(Trifluoromethylsulfonyl)imide and 1-Ethyl-3-methylimidazolium Ethylsulfate. *Applied Spectroscopy* **2007**, *61* (12), 1306-1311. doi: 10.1366/000370207783292000
- (66) Gao, X.; Davies, J. P.; Weaver, M. J., Test of surface selection rules for surface-enhanced Raman scattering: the orientation of adsorbed benzene and monosubstituted benzenes on gold. *The Journal of Physical Chemistry* **1990**, 94 (17), 6858-6864. doi: 10.1021/j100380a059
- (67) Norton, R. D.; Phan, H. T.; Gibbons, S. N.; Haes, A. J., Quantitative Surface-Enhanced Spectroscopy. *Annual Review of Physical Chemistry* **2022**, *73* 141-162. doi: 10.1146/annurev-physchem-082720-033751
- (68) Kornyshev, A. A., Double-Layer in Ionic Liquids: Paradigm Change? *The Journal of Physical Chemistry B* **2007**, *111* (20), 5545-5557. doi: 10.1021/jp0678570
- (69) de Souza, J. P.; Bazant, M. Z., Continuum Theory of Electrostatic Correlations at Charged Surfaces. *The Journal of Physical Chemistry C* **2020**, *124* (21), 11414-11421. doi: 10.1021/acs.jpcc.0c01261
- (70) Bazant, M. Z.; Storey, B. D.; Kornyshev, A. A., Double Layer in Ionic Liquids: Overscreening versus Crowding. *Physical Review Letters* **2011**, *106* (4), 046102. doi: 10.1103/PhysRevLett.106.046102
- (71) Lee, A. A.; Perez-Martinez, C. S.; Smith, A. M.; Perkin, S., Scaling Analysis of the Screening Length in Concentrated Electrolytes. *Physical Review Letters* **2017**, *119* (2), 026002. doi: 10.1103/PhysRevLett.119.026002
- (72) Feaster, J. T.; Shi, C.; Cave, E. R.; Hatsukade, T.; Abram, D. N.; Kuhl, K. P.; Hahn, C.; Nørskov, J. K.; Jaramillo, T. F., Understanding Selectivity for the Electrochemical Reduction of Carbon Dioxide to Formic Acid and Carbon Monoxide on Metal Electrodes. *ACS Catalysis* **2017**, *7* (7), 4822-4827. doi: 10.1021/acscatal.7b00687
- (73) Jiang, B.; Zhang, X.-G.; Jiang, K.; Wu, D.-Y.; Cai, W.-B., Boosting Formate Production in Electrocatalytic CO2 Reduction over Wide Potential Window on Pd Surfaces. *Journal of the American Chemical Society* **2018**, *140* (8), 2880-2889. doi: 10.1021/jacs.7b12506
- (74) McEnaney, J. M.; Blair, S. J.; Nielander, A. C.; Schwalbe, J. A.; Koshy, D. M.; Cargnello, M.; Jaramillo, T. F., Electrolyte Engineering for Efficient Electrochemical Nitrate Reduction to Ammonia on a Titanium Electrode. *ACS Sustainable Chemistry & Engineering* **2020**, *8* (7), 2672-2681. doi: 10.1021/acssuschemeng.9b05983
- (75) Chen, F. Y.; Wu, Z. Y.; Gupta, S.; Rivera, D. J.; Lambeets, S. V.; Pecaut, S.; Kim, J. Y. T.; Zhu, P.; Finfrock, Y. Z.; Meira, D. M.; King, G.; Gao, G.; Xu, W.; Cullen, D. A.; Zhou, H.; Han, Y.; Perea, D. E.; Muhich, C. L.; Wang, H., Efficient conversion of low-concentration nitrate sources into ammonia on a Ru-dispersed Cu nanowire electrocatalyst. *Nature Nanotechnology* **2022**, *17* (7), 759-767. doi: 10.1038/s41565-022-01121-4
- (76) Lim, J.; Liu, C.-Y.; Park, J.; Liu, Y.-H.; Senftle, T. P.; Lee, S. W.; Hatzell, M. C., Structure Sensitivity of Pd Facets for Enhanced Electrochemical Nitrate Reduction to Ammonia. *ACS Catalysis* **2021**, *11* (12), 7568-7577. doi: 10.1021/acscatal.1c01413
- (77) dos Santos, D. P.; Temperini, M. L. A.; Brolo, A. G., Mapping the Energy Distribution of SERRS Hot Spots from Anti-Stokes to Stokes Intensity Ratios. *Journal of the American Chemical Society* **2012**, *134* (32), 13492-13500. doi: 10.1021/ja305580t